Mitigation Schemes for the Reduction of Fretting Wear and Fatigue

2021 IEEE 66th Holm Conference on Electrical Contacts (HLM), DOI: 10.1109/HLM51431.2021.9671166

Huaidong Yang and Itzhak Green
G. W. Woodruff School of Mechanical Engineering
Georgia Institute of Technology
Atlanta, GA 30332-0405, USA
yanghuaidong@gatech.edu and green@gatech.edu[1]

Abstract

Fretting refers to wear damage at the asperities of contacting surfaces. This damage is induced under load and in the presence of repeated relative surface motion. Fretting degrades the surface quality producing increased surface roughness and micropits and cracks, which reduces the fatigue strength of the components. Fretting occurs in many electrical connectors subject to motion (e.g. a printed circuit board connector). Commonly most board-to-board (B2B) electrical connectors are especially vulnerable if there is any relative motion present between the mating connectors. Contact fretting can change the electrical contact resistance of such connectors from milliohms to ohms when vibration is present. Fretting decreases fatigue strength of materials operating under cycling stress. This can result in fretting fatigue, whereby fatigue cracks can initiate in the fretting zone. Then, crack propagate into the material and may cause total elemental failure. Common mitigation strategies rely on adding lubricants to the contact, or making contacts of soft materials. However, such contacts are susceptible to entrapped wear debris. Here a different mitigation strategy is offered that is based on pre-stressing the contacting elements. To mitigate the damage during the fretting motion, two main properties are focused on: plastic strain and wear volume. The plastic strain represents the plastic deformation in the bulk material, which will decrease the life of the component. The wear volume represents the damage at the interface, which will also decrease the life of the component. It is found that pre-stressing may be beneficial for the suppression fretting fatigue, however, if excessive it may increase the plastic strain in the contact.

1. Introduction

Frictional sliding contact analysis provides the foundation of fretting. The theoretical frictional sliding contact analysis is addressed by Johnson [1]. In the elastic regime, he provides solutions of contact pressure, tangential force, and deformations of the contacting surfaces, addressing both cylindrical and spherical contacts in situations of partial and gross slip conditions. The experiments conducted by Courtney-Pratt and Eisner[2] may be of the earliest studies related to the reciprocal frictional sliding phenomenon. They examine the underlying phase of the oscillatory tangential loading applied at the contact between a metallic sphere and metallic flat surfaces. The hysteresis loops of tangential force and the junction growth are indicated by the difference in the electrical conductance.

The early fretting research focused mainly on distinguishing the types of fretting as charted in the fretting map given by Vingsbo and Söderberg [3]. They sort fretting into stick, mixed stick-slip, and gross slip regimes. A mixed fretting regime is then found by Zhou and Vincent [4, 5], as identified from the fretting loop evolution, which varies its shape during thousands of fretting cyclic loadings. A slip index is then introduced by Varenberg et al. [6] to determine the different fretting regimes.

Fretting wear and fretting fatigue have been the two main fretting damages. Fretting wear is the main cause of component failure in the gross slip regime as investigated by Waterhouse [7], McColl et al.[8], Fouvry [9], and Blanchard et al. [10]. Fretting fatigue is the main case of component failure in the partial slip regime as studied by Waterhouse [11], Hills [12], and Szolwinski. [13]. Fouvry, et al. [14] deliver the quantification criteria for different regime of fretting wear and fretting fatigue. Neu et al. [15] build nucleation models to predict fretting fatigue. Later, fretting damage (wear and fatigue) is investigated by increasing the number of loading cycles to the order of thousands or even millions [16-20].

Coatings and lubricant conditions are found to mitigate fretting damage in these works. References [21-23] focus on the fretting damage for materials applied in the steam generator, including Inconel 600, Inconel 690 and Incoloy 800. Tesla Motors reports the use of Inconel instead of steel in electrical contact so it remains springy under the heat of heavy current and increase the maximum pack output from 1300 to 1500 Amps and for longer duration times. However, mitigation methods based on analytical solutions to the fretting phenomenon remain principally unknown.

In the current work, to mitigate the damage caused by fretting, two main properties are focused on - the equivalent plastic strain and the wear volume. The equivalent plastic strain represents the plastic deformation in the bulk material, which will decrease the life of the component. The wear volume represents permanent material removal at the interface, which will also decrease the life or functionality of the component. A designed pre-stress scheme is shown to reduce the equivalent plastic strain, while the analytical solutions derived in the fretting wear model in the previous work [24] helps determine loading condition which avoids maximizing fretting wear volume.

2. Contact Model

The fretting model, as shown in Fig.1, is applicable for both cylindrical and spherical contacts, and used in the current study. For 2D cylindrical contact, the model is between a deformable half cylinder and a deformable flat block. For 3D spherical contact, the model is between a deformable hemisphere and a deformable flat block. A rigid plat is placed on top surface of the upper body to prevent rotation with respect to the Z axis in 2D, and the Y axis in 3D. A normal load in the vertical direction is applied on top surface of the rigid plate. The reciprocal displacement is applied to the top surface of the half cylinder in 2D and hemisphere in 3D. In 3D spherical contact, to reduce the computational effort, the model is cut in half by the X-Z plane. Since the loading condition is symmetric with respect to the X-

[1] Corresponding Author

Z plane, only half of the model needs to be considered in the computational analysis. The roller boundary condition of no displacement normal to the plane are applied to the vertically cut plane of the quarter sphere and to all the five faces of the block, except to the top face, which is free to deform in all directions. The detailed on the fretting model can be found in the work by the author [25]. It is assumed that the heat generated by fretting is relatively small to affect material properties, and that the fretting cycling is quasi-static.

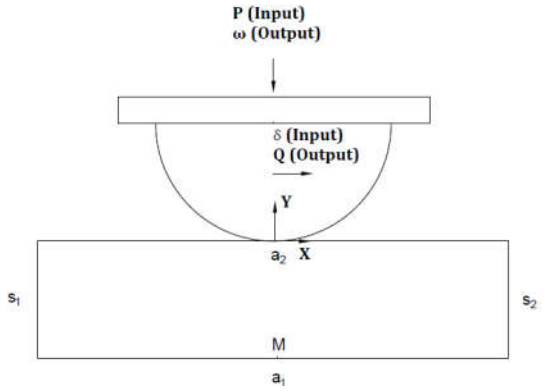

(a) 2D

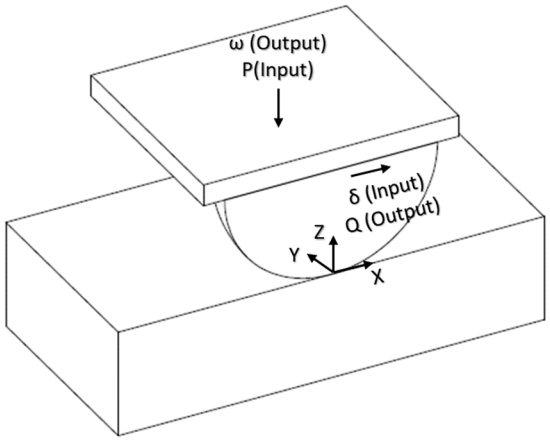

(b) 3D

Figure 1: Schematic of a fretting contact in both 2D and 3D conditions.

The materials of the upper and the bottom bodies are first set to be an identical material pair: Inconel 617/Inconel 617, and then set to be a dissimilar material pair, i.e., Inconel 617/Incoloy 800H. The designation of Inconel 617/Incoloy 800H means that the material of the hemisphere is Inconel 617 and the material of the block is Incoloy 800H. These special alloy choices are promising materials for the structural and in-core components of a high/very high temperature gas cooled reactors (HTGR/VHTRs). However, nondimensionalization shows that the underlying physics holds for any other dissimilar material pairs or length scales. The material properties are listed in Table 1.

An Archard wear model is used at the contact between the contacting bodies,

$$V = \frac{KPS}{H} \quad (1)$$

where V, K, P, S, and H represents the wear volume, dimensionless wear coefficient, normal force, sliding distance, and hardness of the material of interest, respectively. The wear coefficient is set to 10^{-5} without loss of generality[2]. The details of the Archard wear model can be found in the 2D work [24]. It is applied locally (i.e., at each nodal point) at the contact region. The focus in this study is to apply fretting mitigation schemes founded on analytical reasoning and based on these previously built fretting models [24, 25, 27, 28]. The details of mesh convergence are given in the said works and they are not repeated herein.

All the results in this work are normalized by the critical parameters, which are values at the onset of plasticity for pure normal contact. Table 2 lists the critical values for the similar and dissimilar material contact schemes. The derivation of the critical values can be found in [25, 29]. Inconel is an austenitic nickel-chromium-based super alloy that is oxidation and corrosion resistant and is well suited for service in extreme environments, specifically in electrical contacts [30, 31].

3. **Mitigation Methods**

To mitigate the damage during the fretting motion, two main properties are focused upon – the equivalent plastic strain and the wear volume. The equivalent plastic strain represents the plastic deformation in the bulk material, which will decrease the life of the component. The wear volume represents the damage at the interface, which will also decrease the life of the component or its functionality.

3.1 **Pre-stress Scheme**

As shown in Fig.2, in cylindrical contact, before employing the fretting inputs (P and δ), prestressed displacement inputs $S_1 = S_2$ are applied and maintained to two side faces of the bottom block. In this way, the block experiences normal compressive stresses in X direction before the fretting starts, which according to definition of von-Mises stress, it shall elevate the hydrostatic stress situation also during the fretting load.

Table 1. The material properties and critical values for two cases [26].

Temperature	Material	Elastic Modulus[GPa] E	Yield Strength[MPa] S_y	Poisson Ratio ν	C(ν)	$C \cdot S_y$ [MPa]
20°C	Inconel 617	211.0	322	0.3	1.615	520
20°C	Incoloy 800H	196.5	150	0.339	1.662	249

[2] Results will be nondimensionalized, but a numerical value is needed for the FEA numerical execution. For simplicity, it is assumed herein that H=2.8Sy, which may be considered sufficiently accurate for relatively lightly loaded contacts. The hardness, H, can actually vary significantly with the load, as found by Jackson and Green [32].

Table 2. The critical values (onset of plasticity) for different material schemes.

Dimension	Hemisphere Material	Block Material	Critical Interference ω_c [μm]	Critical Load P_c[kN] / Pc/L [kN/m]	Critical Contact Radius/Width a_c/b_c[mm]	Critical Contact Area A_c[mm^2]
2D	Inconel 617	Inconel 617	131	4526	4.99	N/A
2D	Inconel 617	Incoloy 800H	35.6	1053	2.43	N/A
3D	Inconel 617	Inconel 617	24.8	13.472	3.52	38.9
3D	Inconel 617	Incoloy 800H	5.96	1.556	1.73	9.36

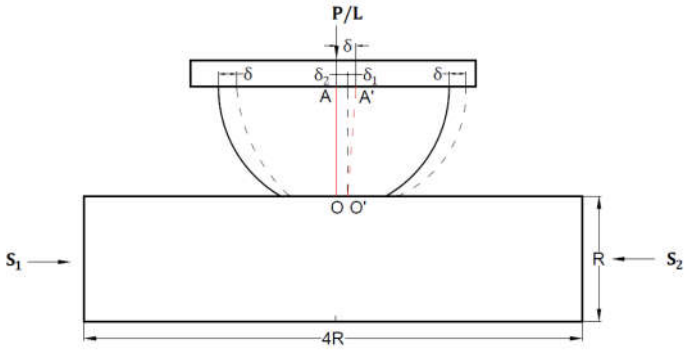

Figure 2: The 2D Pre-stress Scheme.

Figure 3 shows the distribution of equivalent plastic strain at $2P_c$ normal load with different prestress inputs of $S_1 = S_2$ with μ=0.3 after three cycle of fretting motion for Inconel 617/Incoloy 800H. As the prestress input increases from 0 to $6\omega_c$, the plastic strain in the bulk material decreases and then increases. The plastic strain in the bulk material is largest at the centerline when S_1 is small. Thus, the prestress effect elevates the hydrostatic situation, which decreases the plastic strain (Fig.3b and Fig.3c). There are two reasons for that behavior. Firstly, there is σ_z, which elevates the hydrostatic situation, thus reducing the von-Mises stress. Secondly, the negative σ_x opposes the natural tendency of creating a positive σ_x in the fretting sliding motion, which also reduces the von-Mises stress during sliding. With smaller von-Mises stresses, the corresponding plastic strain is smaller. The compressive pre-stress is envisioned to also suppress any crack initiation and/or growth at the two edges of the fretting contact. However, when S_1 increases, the combined effect of shear stress at the two contact edges and the preloaded stress in X direction starts to dominate in the contribution of plastic strain. Thus, in order to reduce the plastic strain in the bulk material, the prestress input cannot be too small or too large.

Moreover, the application of the prestress aggravates the damage at the interface. As shown in Fig.3, the maximum plastic strain always appears at the interface, and it is shown that the maximum plastic strain increases with the prestress input. Since the plastic strain at the interface is a combined effect of frictional shear stress and normal stress, the preloaded stress in the X direction aggravates the shear effect, which increases von Mises stress at the interface.

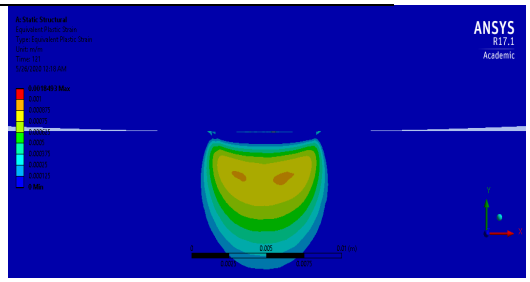

(a) $S_1 = S_2 = 0$ ε_{pmax} =0.0018

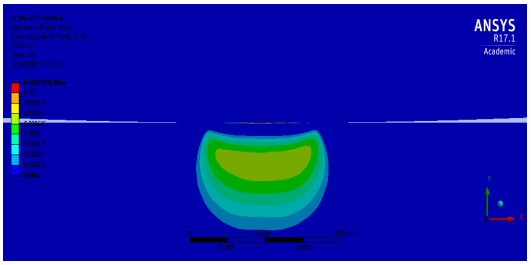

(b) $S_1 = S_2 = 2\omega_c$ ε_{pmax} =0.0037

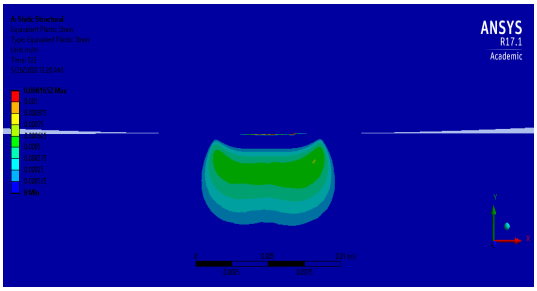

(c) $S_1 = S_2 = 4\omega_c$ ε_{pmax} =0.008

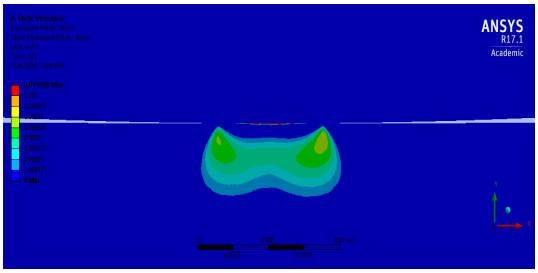

(d) $S_1 = S_2 = 6\omega_c$ ε_{pmax} =0.015

Figure 3: The distribution of equivalent plastic strain at 2Pc normal load with different prestress inputs of S1 and S2 with μ=0.3 after three cycles of fretting motion for Inconel 617/Incoloy 800H, (linear scale: 0-min to 0.004-max).

Similar to the 2D case, in the 3D case, the effect of prestress scheme can also be achieved. In the 3D case, the prestresses can be loaded both in the X (left and right) and Z (front and back) directions. As shown in Fig.4, S_1 and S_2 are inputs in the X direction, while S_3 is in Z direction. It should be noted that the front face is kept at z=0 to maintain symmetric condition with respect to X-Y plane.

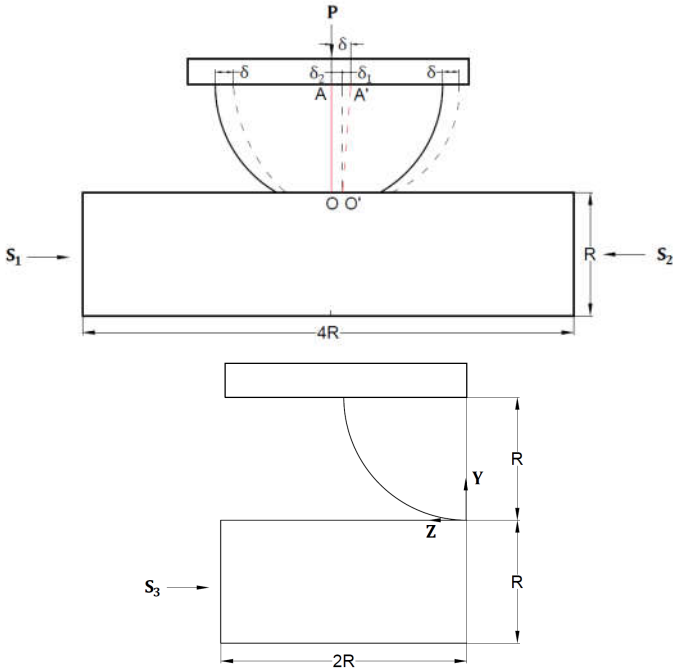

Figure 4: The 3D Pre-stress Scheme in X and Z directions.

Figure 5 shows the distribution of plastic strain at 1.5Pc normal load with different prestress inputs of S_1, S_2, and S_3, with μ=0.3 after three cycles of fretting motion. For the cases with only prestress in X direction (S_3=0), the plastic strain in the bulk material decreases at the centerline when S_1 and S_2 are small (Fig.5b), and the plastic strain near the contact edges starts to increase when S_1 and S_2 are large (Fig.5c). The application of the prestress in both X and Z direction further decreases the plastic strain in the bulk material as shown in Fig.5d. However, the plastic strain at the interface in any case with the prestress scheme is larger than that without prestress scheme, which is indicated by the maximum plastic strain.

3.2 **Fretting Wear**

In the actual working condition, the normal load can be designed to avoid excessive (or maximum) wear. The wear volume for one cycle of fretting can be expressed as a function of the normal load, P, the hardness of the material, H, the wear coefficient, K, the sliding distance at the initiation of gross slip, δ_i, and the wear volume for partial slip partial stick condition, V_0.

$$V = 4V_0 + \frac{4(\Delta-\delta_i)KP}{H} \qquad \delta_i < \Delta \tag{2}$$

By using a constant coefficient of friction (COF), μ, to achieve the effect of friction at the interface, the solutions to δ_i and V_0 can be derived (see [24]). For the 3D spherical contact, the sliding distance at the initiation of gross slip, δ_i, and the wear volume for partial slip partial stick condition, V_0 are derived as given below:

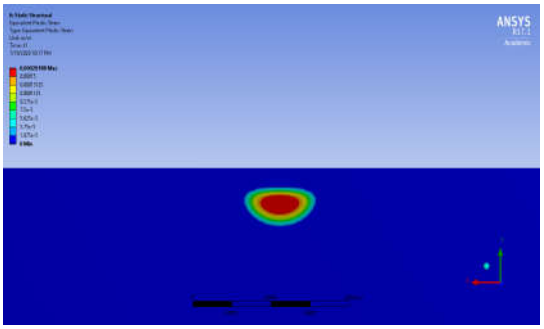

(a) S_1= S_2=0 ε_{pmax} =0.0002

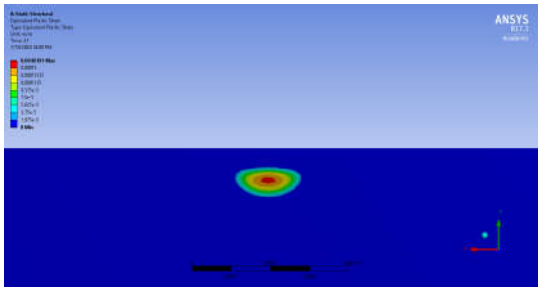

(b) S_1= S_2=1 ω_c ε_{pmax} =0.004

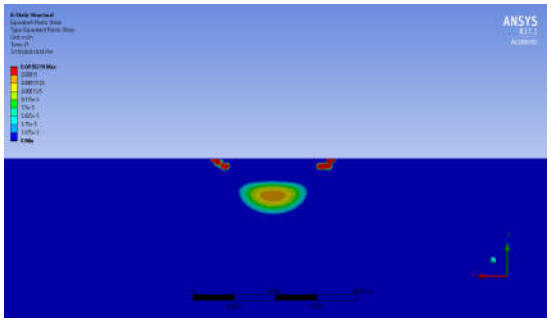

(c) S_1= S_2=1.2 ω_c ε_{pmax} =0.00192

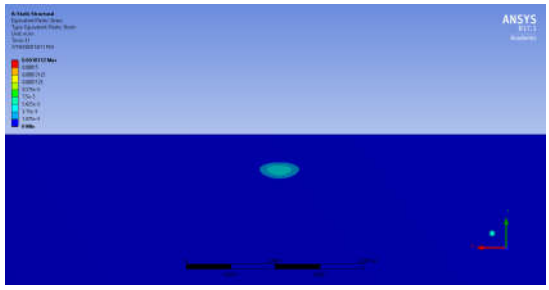

(d) S_1= S_2=1ω_c S_3=2ω_c ε_{pmax} =0.003

Figure 5: The distribution of plastic strain at 1.5P_c normal load with different prestress inputs of S_1, S_2, S_3, and S_4, with μ=0.3 after three cycles of fretting motion (linear scale: 0-min to 0.004-max).

$$\delta_i = \frac{3\mu P}{8a}\left[\frac{(2-\nu_1)(1+\nu_1)}{E_1} + \frac{(2-\nu_2)(1+\nu_2)}{E_2}\right] \tag{3}$$

$$V_0 = \frac{K\pi^2\mu\, p_0^2\, a^3}{60\, H}\left(\frac{2-\nu_1}{G_1}+\frac{2-\nu_2}{G_1}\right) \tag{4}$$

For the 2D cylindrical contact, due to the difficulty of obtaining close form solution, the solutions to the δ_i and V_0 are

only derived for the contact between similar material pairs by using a fitting function. The detailed derivation can be found in [24]. The corresponding equations are given below,

$$\delta_i = 4.78\mu^{1.15}\left(\frac{P/L}{RE}\right)^{0.928}R \tag{5}$$

$$V_0 = \frac{(1-\nu^2)\mu\pi K p_0^2 b^2}{4HE} \tag{6}$$

Suppose that for a certain material pair, the COF is predetermined. As a result, Eq.5-6 (2D) and Eq.3-4 (3D), as derived in this work, can help to determine the worst normal load which would result in the largest wear volume.

As shown in Fig.6 and Fig.7, the wear volume increases with the normal load first but then it decreases. When the normal load is small, the portion of gross slip is relatively large during the entire range of oscillation. Thus, according to the Archard wear law that the wear volume is proportional to the normal load, the wear volume for one general cycle increases. When the normal load is large, the portion of stick and partial slip is relatively large during the entire oscillation. Thus, according to the Archard wear law that the wear volume is proportional to the sliding distance, the wear volume for one general cycle decreases.

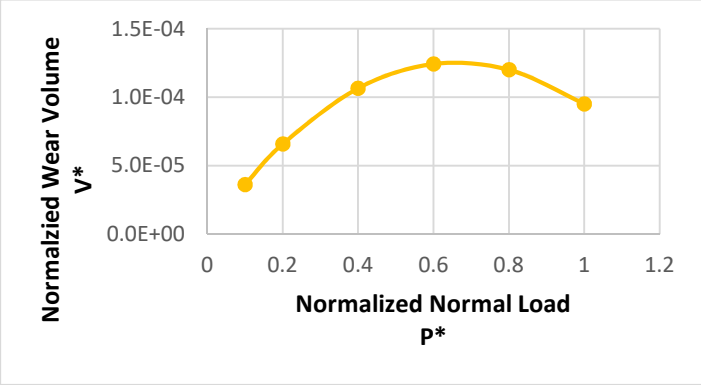

Figure 6: Wear volume of one general cycle in 2D cylindrical contact under different normal load with μ=0.5 and 1ω_c fretting magnitude.

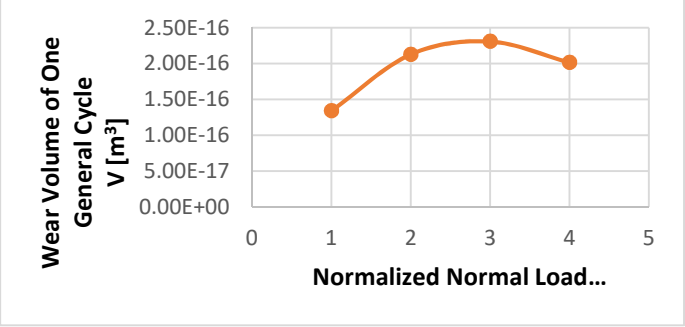

Figure 7: Wear volume of one general cycle in 3D spherical contact under different normal load with μ=0.3 and 1ω_c fretting magnitude.

Based on the observation above, the analytical way to obtain the worst normal load, P_w (i.e., the load that causes maximum wear), is to solve the equation dV/dP=0 for P_w. For the 3D case, the expression of the wear volume is derived in Eqs.2-4. By taking the derivative of Eq.2, the worst normal load, P_w is obtained:

$$P_w = \frac{E_1E_2S}{\mu(-E_2\nu_1^2+E_2\nu_1-E_1\nu_2^2+E_1\nu_2+2E_1+2E_2)} * \sqrt{\frac{6RS(-E_2\nu_1^2-E_1\nu_2^2+E_1+E_2)}{\mu(-E_2\nu_1^2+E_2\nu_1-E_1\nu_2^2+E_1\nu_2+2E_1+2E_2)}} \tag{7}$$

where E_1 and E_2 are elastic moduli, ν_1 and ν_2 are Poisson ratios, μ is COF, R is the equivalent contact radius, and S is the oscillatory sliding magnitude. For similar material pair cases, the P_w can be further simplified to:

$$P_w = \frac{ES}{\mu(-\nu^2+\nu+2)}\sqrt{\frac{3RS(\nu-1)}{2\mu(\nu-2)}} \tag{8}$$

For the 2D case, the expression of the wear volume is derived in Eq.2 and Eqs.5-6. The worst normal load, P_w, is obtained in a similar manner as above. However, a closed form is not feasible. Hence, Pw can be obtained by solving numerically this equation instead.

$$S - 9.216\mu^{1.15}R\left(\frac{P}{RE}\right)^{0.928} - \frac{2\mu P(\nu^2-1)}{\pi E} = 0 \tag{9}$$

To verify Eqs.7-9, the worst normal loads, Pw, that are derived analytically are compared with those obtained numerically for the 2D and 3D cases. The comparison is given in Table 3. For instance, in the 3D dissimilar case, the analytical expression for P_w is derived in Eq. 7, while the dimensional expression of wear volume is derived by Eqs.2-4. In Eq.2, the expression, V(P), is a function of normal load. Numerically, we find the peak of the wear volume and its location, and hence the worst normal load is obtained. These two P_w numerical values are both 0.0044713 MN. Thus, the analytical expression of P_w is verified. Accordingly, based on the results in Table 3, Eqs.7-9 are verified.

Table 3: The worst normal load P_w table from Eqs.7-9 and numerically solving dimensional expression of Eq.2.

	2D (Eq.9 and Eq.2)	3D Dissimilar (Eq.7 and Eq.2)	3D Similar (Eq.7 and Eq.2)
Analytical P_w [MN]	48.446	0.0044713	0.20722
Numerical P_w [MN]	48.445	0.0044713	0.20722

In summary, once the inputs of material properties (E, ν, and μ) and fretting magnitude, S, are determined, P_w can be obtained by Eq. 7-9. From a design point of view, the normal load, P, should be considerably different than P_w, either being much smaller or much larger than the P_w.

4.Conclusion

Two mitigation schemes are proposed, prestress scheme and wear volume mitigation scheme. In the prestress scheme, the plastic strain in the bulk material in reduced at appropriate prestress input, and the prestress in both x and z directions can further reduce the plastic strain in 3D case. There are two reasons for that behavior. Firstly, there is σ_z, which elevates the hydrostatic situation, thus reducing the von-Mises stress. Secondly, the negative σ_x opposes the natural tendency of creating a positive σ_x in the fretting sliding motion, which also reduces the von-Mises stress during sliding. With smaller von-

Mises stresses, the corresponding plastic strain is smaller. The compressive pre-stress is envisioned to also suppress any crack initiation and/or growth at the two edges of the fretting contact. However, the prestress condition aggravates the plastic strain at the interface both in 2D and 3D cases. For engineering purposes, pre-compressed conditions may be achieved locally at the contact also by shot peening. In the wear volume mitigation scheme, the worst normal load can be solved numerically based on Eqs.7-9. From a designer's point of view, the normal load should be either much less or much larger than the P_w.

Acknowledgment

This research is supported by the Department of Energy under Project 2506U87, Award RH452. This support is gratefully acknowledged.

References

[1] Johnson, K. L., and Johnson, K. L., 1987, Contact mechanics, Cambridge university press.

[2] Courtney-Pratt, J., and Eisner, E., 1957, "The effect of a tangential force on the contact of metallic bodies," Proceedings of the Royal Society of London A: Mathematical, Physical and Engineering Sciences, 238(1215), pp. 529-550.

[3] Vingsbo, O., and Söderberg, S., 1988, "On fretting maps," Wear, 126(2), pp. 131-147.

[4] Zhou, Z., and Vincent, L., 1995, "Mixed fretting regime," Wear, 181, pp. 531-536.

[5] Zhou, Z., Nakazawa, K., Zhu, M., Maruyama, N., Kapsa, P., and Vincent, L., 2006, "Progress in fretting maps," Tribology International, 39(10), pp. 1068-1073.

[6] Varenberg, M., Etsion, I., and Halperin, G., 2004, "Slip index: a new unified approach to fretting," Tribology Letters, 17(3), pp. 569-573.

[7] Waterhouse, R., 1984, "Fretting wear," Wear, 100(1-3), pp. 107-118.

[8] McColl, I., Ding, J., and Leen, S., 2004, "Finite element simulation and experimental validation of fretting wear," Wear, 256(11-12), pp. 1114-1127.

[9] Fouvry, S., Kapsa, P., Zahouani, H., and Vincent, L., 1997, "Wear analysis in fretting of hard coatings through a dissipated energy concept," Wear, 203, pp. 393-403.

[10] Blanchard, P., Colombie, C., Pellerin, V., Fayeulle, S., and Vincent, L., 1991, "Material effects in fretting wear: application to iron, titanium, and aluminum alloys," Metallurgical Transactions A, 22(7), pp. 1535-1544.

[11] Waterhouse, R., 1992, "Fretting fatigue," International materials reviews, 37(1), pp. 77-98.

[12] Hills, D. A., 1994, "Mechanics of fretting fatigue," Wear, 175(1-2), pp. 107-113.

[13] Szolwinski, M. P., and Farris, T. N., 1996, "Mechanics of fretting fatigue crack formation," Wear, 198(1-2), pp. 93-107.

[14] Fouvry, S., Kapsa, P., and Vincent, L., 1996, "Quantification of fretting damage," Wear, 200(1-2), pp. 186-205.

[15] Neu, R. W., Pape, J. A., and Swalla, D. R., 2000, "Methodologies for linking nucleation and propagation approaches for predicting life under fretting fatigue," Fretting fatigue: current technology and practices, ASTM International.

[16] Leonard, B. D., Sadeghi, F., Evans, R. D., Doll, G. L., and Shiller, P. J., 2009, "Fretting of WC/aC: H and Cr2N coatings under grease-lubricated and unlubricated conditions," Tribology Transactions, 53(1), pp. 145-153.

[17] Leonard, B. D., Sadeghi, F., Shinde, S., and Mittelbach, M., 2012, "A novel modular fretting wear test rig," Wear, 274, pp. 313-325.

[18] Warhadpande, A., Leonard, B., and Sadeghi, F., 2008, "Effects of fretting wear on rolling contact fatigue life of M50 bearing steel," Proceedings of the Institution of Mechanical Engineers, Part J: Journal of Engineering Tribology, 222(2), pp. 69-80.

[19] Zhu, M., Zhou, Z., Kapsa, P., and Vincent, L., 2001, "Radial fretting fatigue damage of surface coatings," Wear, 250(1-12), pp. 650-657.

[20] Xu, J., Zhu, M., Zhou, Z., Kapsa, P., and Vincent, L., 2003, "An investigation on fretting wear life of bonded MoS2 solid lubricant coatings in complex conditions," Wear, 255(1-6), pp. 253-258.

[21] Kim, D.-G., and Lee, Y.-Z., 2001, "Experimental investigation on sliding and fretting wear of steam generator tube materials," Wear, 250(1-12), pp. 673-680.

[22] Kim, I.-S., Hong, J.-K., Kim, H.-N., and Jang, K.-S., "Wear Behavior of Steam Generator Tubes in Nuclear Power Plant Operating Condition," Proc. Transactions of the 17th International Conference on Structural Mechanics in Reactor Technology (SMiRT 17), Prague, Czech Republic, pp. D04-05.

[23] Zhang, X.-Y., Liu, J.-H., Cai, Z.-B., Peng, J.-F., Zhu, M.-H., and Ren, P.-D., 2017, "Experimental Study of the Fretting Wear Behavior of Incoloy 800 Alloy at High Temperature," Tribology Transactions, pp. 1-10.

[24] Yang, H., and Green, I., 2019, "Fretting Wear Modeling of Cylindrical Line Contact in Plane-Strain Borne by the Finite Element Method," Journal of Applied Mechanics, 86(6).

[25] Yang, H., and Green, I., 2019, "Analysis of Displacement-Controlled Fretting Between a Hemisphere and a Flat Block in Elasto-Plastic Contacts," Journal of Tribology, 141(3).

[26] METALS, S., 2008, "PRODUCT HANDBOOK OF HIGHPERFORMANCE NICKEL ALLOYS,"Product Handbook.

[27] Yang, H., and Green, I., 2018, "An elastoplastic finite element study of displacement-controlled fretting in a plane-strain cylindrical contact," Journal of Tribology, 140(4).

[28] Yang, H., and Green, I., 2019, "A fretting finite element investigation of a plane-strain cylindrical contact of Inconel 617/Incoloy 800H at room and high temperatures," Proceedings of the Institution of Mechanical Engineers, Part J: Journal of Engineering Tribology, 233(4), pp. 553-569.

[29] Yang, H., and Green, I., 2020, "An elastoplastic finite element study of cylindrical plane-strain contact for steel/steel and Inconel 617/Incoloy 800H undergoing unidirectional sliding," Proceedings of the Institution of Mechanical Engineers, Part J: Journal of Engineering Tribology, 234(1), pp. 126-133.

[30] Pal, S.K., Son, Y., Borca-Tasciuc, T. *, 2008,* Thermal and electrical transport along MWCNT arrays grown on Inconel substrates. *Journal of Materials Research* **23,** 2099–2105 (2008). https://doi.org/10.1557/JMR.2008.0256.

[31] Geun Dong Song, Jeoh Han, Soon-Hyeok Jeon, and Do Haeng Hur, 2019, "Stress Corrosion Cracking Behavior of Alloy 600 Coupled to Magnetite under High-Temperature Caustic Conditions," Materials 2019 Jul; 12(13): 2091, doi: 10.3390/ma12132091

[32] Jackson, R. L., and Green, I., "A Finite Element Study of Elasto-plastic Hemispherical Contact Against a Rigid Flat," ASME Trans., Journal of Tribology, Vol. 127, No. 2, (April 2005), 343-354.